NANO LETTERS

Letter

pubs.acs.org/NanoLett

Enhanced Anisotropic Effective *g* Factors of an $Al_{0.25}Ga_{0.75}N$/GaN Heterostructure Based Quantum Point Contact

Fangchao Lu,[†] Ning Tang,*[,†] Shaoyun Huang,[‡] Marcus Larsson,[§,⊥] Ivan Maximov,[§] Mariusz Graczyk,[§] Junxi Duan,[†] Sidong Liu,[†] Weikun Ge,[†,∥] Fujun Xu,[†] and Bo Shen*[,†]

[†]State Key Laboratory of Artificial Microstructure and Mesoscopic Physics, School of Physics, Peking University, Beijing 100871, People's Republic of China

[‡]Key Laboratory for the Physics and Chemistry of Nanodevices and Department of Electronics, Peking University, Beijing 100871, People's Republic of China

[§]Division of Solid State Physics, Lund University, S-22100 Lund, Sweden

[∥]Department of Physics, Tsinghua University, Beijing 100084, People's Republic of China

Supporting Information

ABSTRACT: Gate-defined quantum point contacts (QPCs) were fabricated with $Al_{0.25}Ga_{0.75}N$/GaN heterostructures grown by metal−organic chemical vapor deposition (MOCVD). In the transport study of the Zeeman effect, greatly enhanced effective *g* factors (*g**) were obtained. The in-plane *g** is found to be 5.5 ± 0.6, 4.8 ± 0.4, and 4.2 ± 0.4 for the first to the third subband, respectively. Similarly, the out-of-plane *g** is 8.3 ± 0.6, 6.7 ± 0.7, and 5.1 ± 0.7. Increasing *g** with the population of odd-numbered spin-splitted subbands are obtained at 14 T. This portion of increase is assumed to arise from the exchange interaction in one-dimensional systems. A careful analysis shows that not only the exchange interaction but the spin−orbit interaction (SOI) in the strongly confined QPC contributes to the enhancement and anisotropy of *g** in different subbands. An approach to distinguish the respective contributions from the SOI and exchange interaction is therefore proposed.

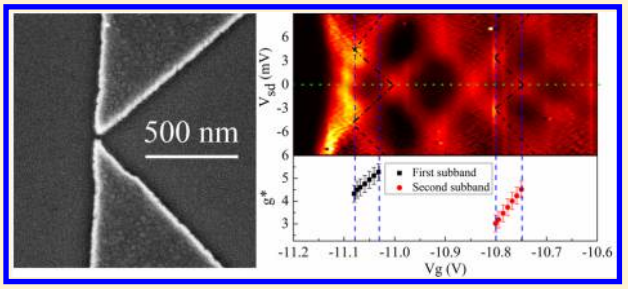

KEYWORDS: *Quantum point contacts (QPCs), $Al_{0.25}Ga_{0.75}N$/GaN heterostructures, effective g factor, spin−orbit interaction (SOI), exchange interaction*

The electron-spin degree of freedom in nanometer-scaled structures has aroused great interests due to potential applications in quantum information processing technologies.[1,2] One ingredient in realizing the quantum processing functionalities is the ability to manipulate the spin electrically therein. This is applicable in a strong spin−orbit interaction (SOI) system. The SOI in nanostructures results in a fluctuation and anisotropy of the effective Landé *g*-factor (also denoted as *g**) in different energy levels.[3−7] Recent studies further show that the electron−electron interaction also plays a similar role on the modification of *g** in low-dimensional systems.[8,9] So far, the contributions to *g** from such two interactions have yet been studied comprehensively. In this work, quantum point contacts (QPCs) with both strong SOI and strong electron−electron interaction are designed and fabricated in $Al_xGa_{1-x}N$/GaN heterostructures, in order to clarify the two contributions at low temperatures by experimentally measuring *g** from the Zeeman effect of opposite spins in a magnetic field.

In comparison to GaAs, GaN is expected to possess stronger electron−electron interactions, due to larger electron effective mass $m^* = 0.2m_e$ and smaller dielectric constant $\varepsilon = 9$. In addition, in both GaN and $Al_xGa_{1-x}N$, the reduced symmetry of the wurtzite crystal structure results in a large spontaneous polarization. Moreover, the lattice mismatch of GaN and $Al_xGa_{1-x}N$ causes a piezoelectric field at the heterointerface. Both polarization fields are as large as a few MV/cm, giving rise to a large Rashba SOI,[10,11] which can be further tuned by an external electric field and provides a convenient electrical modulation on *g**. It has been shown that the SOI in the heterostructure is positively proportional to the Al content in the $Al_xGa_{1-x}N$ barrier layer.[12] This fact allows us to design appropriate device structures based on $Al_xGa_{1-x}N$/GaN heterostructures. In this work, the Al content of $x = 0.25$ was adopted to obtain a large built-in electric field pointing to the substrate, while holding a high quality surface and a high two-dimensional electron gas (2DEG) mobility. In such materials, the Rashba coefficient is obtained to be $\alpha = 2.6 \times 10^{-12}$ eV m, and the spin splitting caused by Rashba SOI is as large as 3.7 meV.[13]

The $Al_{0.25}Ga_{0.75}N$/GaN heterostructures were prepared by means of metal−organic chemical vapor deposition (MOCVD) methods on *c*-plane sapphire substrates. The growth processes

Received: May 15, 2013
Revised: August 31, 2013
Published: September 16, 2013

were initiated by a 20-nm-thick nucleation layer at 530 °C, followed by the growth of a 2-μm-thick unintentionally doped GaN (i-GaN) buffer layer at 1060 °C. Subsequently, a 1-nm-thick AlN interlayer and a 25-nm-thick unintentionally doped $Al_{0.25}Ga_{0.75}N$ barrier was grown at 1085 °C. The layer structures are shown schematically in Figure 1 a. The two-dimensional

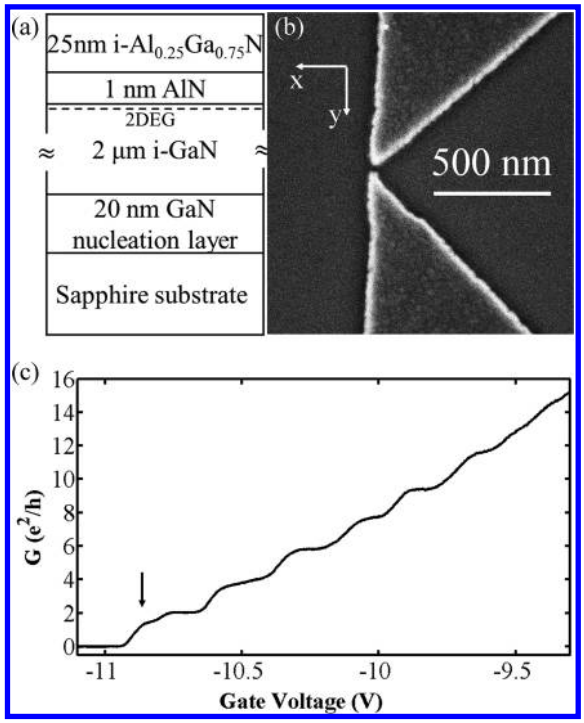

Figure 1. (a) Schematic layer structures of the $Al_{0.25}Ga_{0.75}N$/GaN heterostructure; (b) a representative SEM image of a QPC fabricated in the same batch, with the definition of the coordinates; (c) conductance G of the QPC device measured as a function of V_g at V_{sd} = 100 μV.

electron density and mobility are $n = 1.0 \times 10^{13}$ cm^{-2} and $\mu = 1.1 \times 10^4$ cm^2/(V s), respectively, extracted from the Hall measurements at 1.3 K. The high carrier concentration is induced by the large built-in electric field.

Device fabrications of QPCs started from the heterostructure mesas defined by photolithography and inductively coupled plasma (ICP) etching techniques. Etching down 2.0 μm deep to the sapphire substrate was employed to avoid parallel conductions in the i-GaN layer. Ohmic contacts of the 2DEG were realized by Ti/Al/Ni/Au multiple layered metal electrodes with thickness of 20/150/35/200 nm and a rapid annealing at 850 °C for 45 s in a N_2 ambient. In order to passivate the $Al_{0.25}Ga_{0.75}N$ surface for stable gate performance, the sample was then treated in the solution of [$(NH_4)_2S_x/H_2O$ = 1:9] at 60 °C for 20 min right before the gate dielectric deposition. A 24-nm-thick high-κ HfO_2 thin film, deposited by atomic layer deposition (ALD) at 100 °C, was employed as the gate dielectric to suppress gate leakage and to keep an effective gating performance. The mesas were patterned in another photolithography process to prepare large bonding pads by using Ti/Au with thickness of 5/200 nm. [See Figure S1, Supporting Information, for the SEM image of the mesa after the previous steps.] Split gates with an opening of 60 nm, defined by electron-beam lithography, metal evaporation of 5-nm-Ti/45-nm-Au, and liftoff techniques, were extended to the bonding pads. Figure 1b shows a scanning electron microscope (SEM) image of a representative QPC with a schematic electrical measurement setup.

The QPC was studied by dc measurements in a ^{4}He cryostat at 1.3 K. [See Figure S2, Supporting Information, for the schematic of the measurement setup.] The series resistance of QPC, arising from connection cables, pad contacts, and 2DEG body, was obtained to be 450 Ω at zero gate voltage (V_g). At a nonzero V_g, the resistance of the QPC is derived by subtracting that series term from the total resistance. When V_g is swept negatively toward pinch-off, the resistance of the QPC drastically increases due to depletion effect. Around −10 V of V_g, a few numbers of remained conduction paths (one-dimensional subbands) can be observed in light of well-resolved quantized conductance plateaus at the height of $2n \times e^2/h$, as shown in Figure 1c. Here, n represents the nth subband, e the elemental charge of electron, and h the Plank's constant. The differential conductance ($G = dI_{sd}/dV_{sd}$) was obtained by numerical method. Here, V_{sd} is the source-drain voltage and I_{sd} the source-drain current. It is worthwhile to mention that a 0.7 structure shoulder[14,15] was found as indicated by an arrow but excluded from our following discussions in the present letter.

In order to highlight the changes of the conductance, dG/dV_g as functions of V_{sd} and V_g is shown in Figure 2, in which

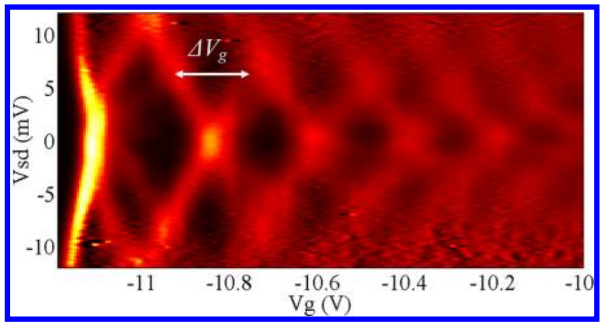

Figure 2. Numerical dG/dV_g of the QPC as functions of both V_{sd} and V_g. An example of ΔV_g is indicated by the white arrowed line.

the transition regions between conductance plateaus are depicted by peaks and represented by bright lines. A lever arm factor a_n correlates a change of V_g ($\Delta V_{g,n}$) to the corresponding nth energy level's shift ($\Delta V_{sd,n}$). In concrete, for the nth subband, the lever arm factor is extracted as follows:[16]

$$\alpha_n = d(V_{sd,n})/d(\Delta V_{g,n}) \quad (1)$$

In Figure 2, the dimension of the diamond structured regions indicates an energy separation between neighboring subbands. Accordingly, the energy spacing between the first and second energy levels is 11 meV. We attribute this large orbital energy to the strong confinement of the one-dimensional (1D) channel.

Magnetotransport characteristics were investigated in a linear response region at a *dc* bias of V_{sd} = 100 μV with a magnetic field B applied from 0 to 14 T along the directions parallel to the current (in-plane orientation defined as the x-axis) and perpendicular to the 2DEG (the out-of-plane orientation defined as the z-axis). In a nonzero magnetic field, each spin degenerated 1D subband opens an energy gap by $E_z = g^*\mu_B B$ due to Zeeman effect, where E_z is the Zeeman splitting energy and μ_B the Bohr magneton. As a consequence of the spin degeneration lifting, each of the $2e^2/h$ conductance plateaus

dx.doi.org/10.1021/nl401724m | Nano Lett. 2013, 13, 4654−4658

evolves into two subplateaus with a height of e^2/h, and the spin-up and -down levels shift oppositely in the colormap plot of transconductance in Figures 3a,b. When B is along the x-axis as

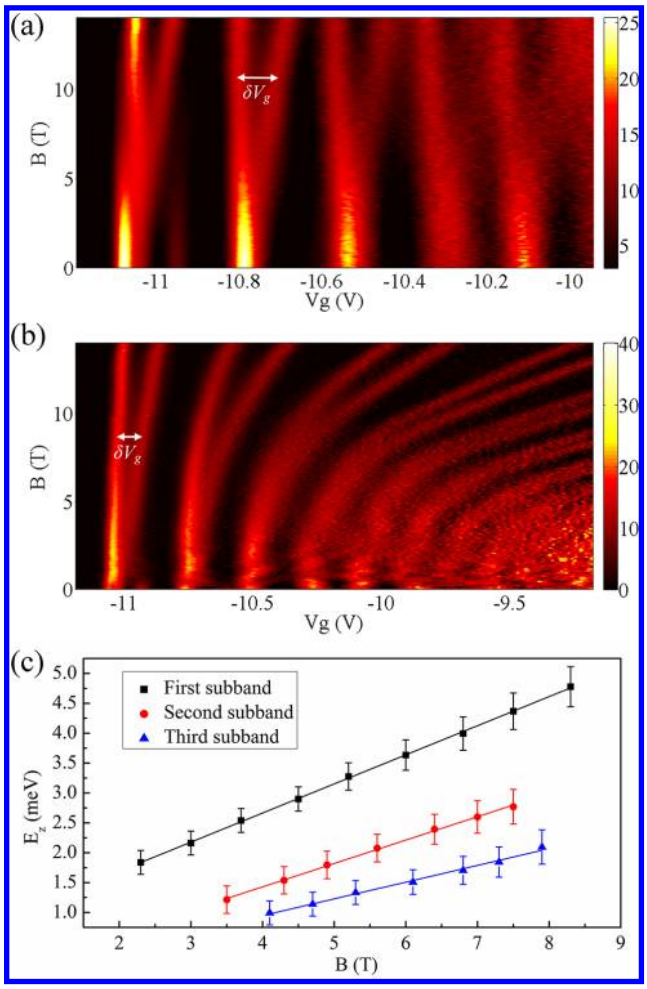

Figure 3. (a) Transconductance of the QPC as functions of V_g and the magnetic field B applied along the direction of the current (x-axis). (b) Transconductance of the QPC as functions of V_g and the magnetic field B applied perpendicular to the 2DEG (z-axis). Both measurements were carried out at V_{sd} = 100 μV. In both figures, bright lines indicate the peaks of dG/dV_g, and the unit for the color bar is (e^2/h) V^{-1}. Examples of ΔV_g are indicated by the white arrowed lines. (c) The Zeeman splitting energy of the first three subbands obtained in the magnetic field along the z-axis as a function of B. The square, circle, and triangular legends denote the first, second, and third subbands, respectively.

indicated in Figure 3a, the splitting along the gate voltage corresponds to the two levels of spin-up and -down evolving linearly in opposite directions. The Zeeman splitting energy can be obtained by using the lever arm factor derived from eq 1, and thus g^* can be obtained as

$$g^*_n = \alpha_n \frac{e}{\mu_B} \frac{d(\delta V_{g,n})}{dB} \quad (2)$$

The first three subbands turn out to have $g^*_{1,x}$ = 5.5 ± 0.6, $g^*_{2,x}$ = 4.8 ± 0.4, and $g^*_{3,x}$ = 4.2 ± 0.4. When B is along z-axis, the magnetic potential gives rise to an extra parabolic confinement to the Hamiltonian. Consequently, an extra orbital energy is added to the nth energy level, leading to magnetic depopulation, as shown by the bending of each energy level toward positive gate voltage in Figure 3b.[17] Such bending does not change the Zeeman splitting of each subband so that δV_g keeps linearly proportional to B in low magnetic fields (below 8 T). The Zeeman splitting energies of the first, second, and third subbands as a function of B in this region are shown in Figure 3c, and $g^*_{1,z}$ = 8.3 ± 0.6, $g^*_{2,z}$ = 6.7 ± 0.7, and $g^*_{3,z}$ = 5.1 ± 0.7 are calculated as well. In a higher magnetic field, the carrier concentration varies much with B due to the magnetic depopulation, giving rise to a considerable change of the lever arm factor with V_g. Therefore, the curves in Figure 3c may deviate from a linear trend in a higher B. It is worthwhile to mention that, in Figure 3a, the curves also bend a little bit toward the positive gate voltage because the 2DEG defined by the triangular well at the heterointerface has finite thickness; therefore, it also goes through a negligible magnetic depopulation in the in-plane B. However, such bending effect is trivial to be considered in the calculation of g^*.

The g^* of QPC in this work shows prominent anisotropy, and in both field orientations, g^* is greatly enhanced compared with g^* = 2.06 as obtained in GaN/AlGaN 2DEGs.[18] For electrons confined along z-axis in a quantum well, in the Kane model taking into account the SOI, the couplings of energy bands have individually different contributions to the in-plane and out-of-plane g factors, giving rise to a larger out-of-plane g factor than the in-plane one.[19,20] In $Al_{0.25}Ga_{0.75}N$/GaN heterostructures, the strong Rashba SOI leads to a clear anisotropy of the g factors. When the angle between the magnetic field and the 2DEG normal is decreased, g^* gets larger as it tends to the out-plane value.[21] As such, it is reasonable to speculate that the extra lateral confinement could further add to the anisotropy of g^* in the 1D subbands of QPCs. Theoretical studies proved that in a model of rectangular quantum wire, both the value and anisotropy of g^* are modified by lateral confinement.[5] Experimentally, in a QPC based on MBE-grown $Al_{0.06}Ga_{0.94}N$/GaN heterostructures, Chou et al. obtained g^* = 2.55 in the first subband.[22] The more remarkable enhancement effect shown in this work may result from a much larger Al ratio (0.25 vs 0.06) and a smaller opening of QPC (60 nm vs 80 nm), proving the point that g^* benefits from a large Rashba SOI in quantum confined systems. The large Rashba SOI is induced by the high Al ratio, which also has a positive correlation with both the band offset and the polarization field in heterostructures. The width of the triangular quantum well is narrowed by large band offset and polarization field; consequently, in $Al_{0.25}Ga_{0.75}N$/GaN heterostructures, the quantum well is as narrow as a few nanometers. Given the much smaller size of our QPC, the electrons in it are more confined compared with that in ref 22. Furthermore, the confinement potential from V_g gives rise to an additional structure inversion asymmetry (SIA), which modifies the band structure and dispersion relationship of the electrons. Such effect gets more important as 1D channels are narrowed, adding to the enhancement and the anisotropy of g^*.[23,24] SOI in AlGaAs/GaAs heterostructures is smaller than in $Al_{0.25}Ga_{0.75}N$/GaN heterostructures. In AlGaAs/GaAs QPCs, g^* is found to be enhanced from 0.44 for 2DEGs to a value ranging from 1.1 to 1.3 for the first 1D subband,[14,16] the enhancement of which are less than g^* in this work.

Besides the SOI, it is suggested that the electron−electron interactions can also give rise to an enhancement of g^*, which can be reflected in the dependence of g^* upon the filling status of the 1D subbands.[8] As described below, this can be analyzed

dx.doi.org/10.1021/nl401724m | Nano Lett. 2013, 13, 4654−4658

by the stability diagram of spin-splitted subbands. At $V_{sd} \approx 0$, the Fermi level (E_F) in the QPC is as high as the chemical potential of the source and drain reservoirs, denoted as μ_s and μ_d, respectively. When an external magnetic field is applied, the spin-up ($\mu_\uparrow$) and -down ($\mu_\downarrow$) levels would be well separated by the Zeeman splitting energy E_z. The value of E_z used in the above calculation is derived from two specific gate voltages at which either $\mu_\uparrow$ or $\mu_\downarrow$ level lines up with μ_s and μ_d. The g^* obtained by this way is, in fact, at a specific filling status, i.e., the $\mu_\downarrow$ level of the identical subband just being lined up with E_F, as shown by the inset indicating Mark-F in the middle panel of Figure 4a. In a general case, E_z is considered to depend on the

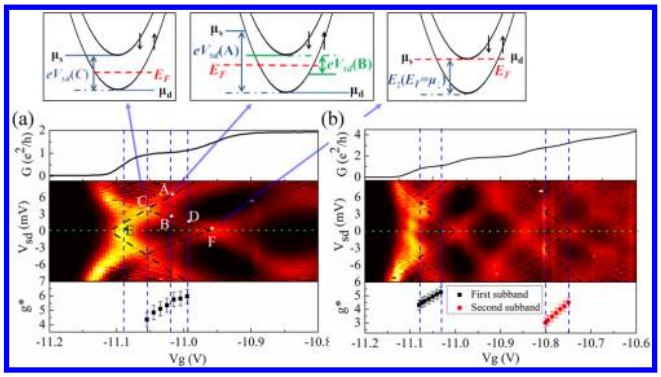

Figure 4. (a) Middle panel shows the stability diagram at 14 T in perpendicular magnetic field (z-axis), and the upper panel shows the V_g dependences of conductance along the green dotted line-cut at $V_{sd} = 0$. The bottom panel is g^* of the first subband as a function of V_g. The three insets illustrate the configuration of the subbands at Marks-C, -F, and -A (-B), as indicated by the arrows. (b) The middle panel shows the stability diagram at 14 T in the in-plane magnetic field (x-axis). The upper panel shows the V_g dependences of conductance along the green dotted line-cut at $V_{sd} = 0$. The bottom panel is g^* of the first and second subbands as a function of V_g.

filling status of the two spin levels, i.e., the position of E_F with respect to $\mu_\uparrow$ and $\mu_\downarrow$. To clarify this point, we made further measurements to obtain the stability diagram at a magnetic field of 14 T for both B orientations. We would like to point out that if E_z (or g^*) is derived from the lever arm factor α, the discussion should be limited in low magnetic fields for the negligible magnetic depopulation effect; however, if α is not involved in the derivation, such limitation is not necessary. The stability diagrams in the in-plane and out-of-plane fields are shown in the middle panels of Figures 4a,b, respectively. For a specific subband, e.g., the first one, the dashed (dash dotted) lines represent the positions where the spin-up (-down) level is aligned with either the source or drain reservoir. The crossing of the two lines, e.g., Mark-C in the middle panel of Figure 4a, represents the situation that E_F lies in the middle of the two spin levels ($\mu_\uparrow$ and $\mu_\downarrow$). When E_F moves toward either $\mu_\uparrow$ or $\mu_\downarrow$, certain V_{sd} is required to allow either μ_s or μ_d to align back with either of the spin levels, as illustrated by Marks-A and -B. Thus, E_z can be extracted for each V_g as $E_z = [V_{sd}(A) + V_{sd}(B)]/2$, and $g^*(V_g)$ in both B orientations can be calculated as well. g^* for the first subband in perpendicular B and for the first two subbands in parallel B is shown in the bottom panels of Figures 4a,b, respectively. An increased g^* with V_g for each subband can be found, as electrons are populated from $\mu_\uparrow$ to $\mu_\downarrow$ of the identical subband.

The above observed results are assumed to be induced by the exchange interaction in the one-dimensional system. Whenever E_F reaches the $\mu_\uparrow$ level, the spin polarization effects take place and become larger as the E_F continues to gradually move to the $\mu_\downarrow$ level. The spin polarization effect leads to an exchange effect, which repels the spin-up and -down levels of the identical 1D subband toward opposite directions, resulting in an increasing g^* with rising E_F. We note here that Mark-D corresponds to the status that E_F lies a little bit lower than $\mu_\downarrow$. Up to Mark-F where E_F reaches $\mu_\downarrow$, g^* should further increase from $g^*(D)$ to the above-mentioned $g^*(F)$, which was obtained using δV_g and the lever arm α. A good consistency can be found between g^* calculated by the two methods, proving that an enhancement induced by the exchange interaction does exist in the previously obtained g^*. Noticeably, at Mark-E where E_F aligns with $\mu_\uparrow$, the g^* is dominated by the SOI, which is actually already larger than that in $Al_xGa_{1-x}N$/GaN 2DEGs. With E_F approaching the $\mu_\downarrow$ level, the enhancement of g^* is dominantly contributed by the exchange interaction, which is suggested to be anisotropic with large SIA.[25]

In summary, a large Rashba SOI was realized in a quasi-1D QPC fabricated on MOCVD-grown $Al_{0.25}Ga_{0.75}N$/GaN heterostructures. The effective Landé factor g^* of the first three subbands was extracted from Zeeman effect in two magnetic field orientations, arriving at $g^*_{1,x} = 5.5 \pm 0.6$, $g^*_{2,x} = 4.8 \pm 0.4$, and $g^*_{3,x} = 4.2 \pm 0.4$ as well as $g^*_{1,z} = 8.3 \pm 0.6$, $g^*_{2,z} = 6.7 \pm 0.7$, and $g^*_{3,z} = 5.1 \pm 0.7$. The enhanced g^* is anisotropic and increases as the lateral confinement becomes stronger. Both the large Rashba SOI and the exchange interaction in the 1D system contribute to this enhancement. g^* within each subband is further found to increase with the population of odd-numbered spin-splitted subbands, due to the exchange interaction only. One may thereby clarify the two contributions qualitatively and quantitatively. In addition, the nanodevices fabricated on $Al_xGa_{1-x}N$/GaN heterostructures with great polarization-induced built-in electric field could find prospective applications on electron-spin manipulations for quantum information processing.

■ ASSOCIATED CONTENT

Supporting Information

Additional information and figures. This material is available free of charge via the Internet at http://pubs.acs.org.

■ AUTHOR INFORMATION

Corresponding Authors

*(N.T.) E-mail: ntang@pku.edu.cn.

*(B.S.) E-mail: bshen@pku.edu.cn.

Present Address

⊥Department of Applied Physics, University of Tokyo, Bunkyo-ku, Tokyo 113-8656, Japan.

Notes

The authors declare no competing financial interest.

■ ACKNOWLEDGMENTS

This work was supported by National Basic Research Program of China (Nos. 2012CB619306, 2013CB921901, and 2012CB921304), the National Natural Science Foundation of China (Nos. 61376095, 11174008, and 60990313), and the Wuhan National High Magnetic Field Center (WHMFCKF2011004).

■ REFERENCES

(1) Loss, D.; DiVincenzo, D. P. *Phys. Rev. A* **1998**, *57* (1), 120.

(2) DiVincenzo, D. P.; Bacon, D.; Kempe, J.; Burkard, G.; Whaley, K. B. *Nature* **2000**, *408*, 339.
(3) Gelabert, M. M.; Serra, L. *Phys. Rev. B* **2011**, *84* (7), 075343.
(4) Kiselev, A.; Ivchenko, E.; Rössler, U. *Phys. Rev. B* **1998**, *58* (24), 16353.
(5) Koduvayur, S.; Rokhinson, L.; Tsui, D.; Pfeiffer, L.; West, K. *Phys. Rev. Lett.* **2008**, *100* (12), 126401.
(6) Valín-Rodríguez, M.; Puente, A.; Serra, L. *Phys. Rev. B* **2004**, *69* (8), 085306.
(7) Takahashi, S.; Deacon, R. S.; Yoshida, K.; Oiwa, A.; Shibata, K.; Hirakawa, K.; Tokura, Y.; Tarucha, S. *Phys. Rev. Lett.* **2010**, *104* (24), 246801.
(8) Wang, C. K.; Berggren, K. F. *Phys. Rev. B* **1996**, *54* (20), 14257−14260.
(9) Martin, T.; Szorkovszky, A.; Micolich, A.; Hamilton, A.; Marlow, C.; Linke, H.; Taylor, R.; Samuelson, L. *Appl. Phys. Lett.* **2008**, *93*, 012105.
(10) Bernardini, F.; Fiorentini, V.; Vanderbilt, D. *Phys. Rev. B* **1997**, *56* (16), R10024.
(11) Ambacher, O.; Smart, J.; Shealy, J.; Weimann, N.; Chu, K.; Murphy, M.; Schaff, W.; Eastman, L.; Dimitrov, R.; Wittmer, L. *J. Appl. Phys.* **1999**, *85* (6), 3222−3233.
(12) Tang, N.; Shen, B.; Han, K.; Lu, F. C.; Xu, F. J.; Qin, Z. X.; Zhang, G. Y. *Appl. Phys. Lett.* **2008**, *93* (17), 172113.
(13) Yin, C.; Shen, B.; Zhang, Q.; Xu, F.; Tang, N.; Cen, L.; Wang, X.; Chen, Y.; Yu, J. *Appl. Phys. Lett.* **2010**, *97* (18), 181904.
(14) Thomas, K. J.; Nicholls, J. T.; Simmons, M. Y.; Pepper, M.; Mace, D. R.; Ritchie, D. A. *Phys. Rev. Lett.* **1996**, *77* (1), 135−138.
(15) Cronenwett, S. M.; Lynch, H. J.; Goldhaber-Gordon, D.; Kouwenhoven, L. P.; Marcus, C. M.; Hirose, K.; Wingreen, N. S.; Umansky, V. *Phys. Rev. Lett.* **2002**, *88* (22), 226805.
(16) Patel, N. K.; Nicholls, J. T.; Martn-Moreno, L.; Pepper, M.; Frost, J. E. F.; Ritchie, D. A.; Jones, G. A. C. *Phys. Rev. B* **1991**, *44* (19), 10973−10975.
(17) Berggren, K. F.; Thornton, T. J.; Newson, D. J.; Pepper, M. *Phys. Rev. Lett.* **1986**, *57* (14), 1769−1772.
(18) Knap, W.; Frayssinet, E.; Sadowski, M.; Skierbiszewski, C.; Maude, D.; Falko, V.; Khan, M. A.; Shur, M. *Appl. Phys. Lett.* **1999**, *75* (20), 3156−3158.
(19) Winkler, R. *Spin−Orbit Coupling Effects in Two-Dimensional Electron and Hole Systems*; Springer: New York, 2003; pp 131−150.
(20) Ivchenko, E.; Kiselev, A.; Willander, M. *Solid State Commun.* **1997**, *102* (5), 375−378.
(21) Ning, T.; Kui, H.; Fang-Chao, L.; Jun-Xi, D.; Fu-Jun, X.; Bo, S. *Chin. Phys. Lett.* **2011**, *28* (3), 037103.
(22) Chou, H.; Lüscher, S.; Goldhaber-Gordon, D.; Manfra, M.; Sergent, A.; West, K.; Molnar, R. *Appl. Phys. Lett.* **2005**, *86*, 073108.
(23) Moroz, A.; Barnes, C. *Phys. Rev. B* **1999**, *60* (20), 14272.
(24) Pershin, Y. V.; Nesteroff, J. A.; Privman, V. *Phys. Rev. B* **2004**, *69* (12), 121306.
(25) Kavokin, K. V. *Phys. Rev. B* **2004**, *69* (7), 075302.